Length dependence of quantized conductance in ballistic constrictions fabricated on InAs/AlSb quantum wells

S. J. Koester,* B. Brar, C. R. Bolognesi, E. J. Caine, A. Patlach, E. L. Hu, and H. Kroemer
Department of Electrical and Computer Engineering, University of California at Santa Barbara, Santa Barbara, California 93106

M. J. Rooks
Cornell Nanofabrication Facility, Cornell University, Ithaca, New York 14853
(Received 15 May 1995; revised manuscript received 18 January 1996)

A length-dependent analysis of quantized conductance in split-gate constrictions fabricated on InAs/AlSb quantum-well heterostructures is presented. Conductance steps with spacing within a few percent of $2e^2/h$ are observed in constrictions with channel lengths of 0.2 μm. With increasing constriction length nearly ideal quantized conductance can still be observed, even in constrictions as long as 2.0 μm. The values of the quantized step heights are found to vary more from device to device with increasing length. Our length-dependent data differ considerably from previous reports on GaAs/Al_xGa_{1-x}As split-gate devices where the quantized conductance was severely degraded for constriction lengths $\gtrsim$ 0.6 μm. Temperature-dependent measurements indicate that the 2.0-μm-long devices have one-dimensional (1D) subband spacings close to 10 meV. The improved length performance of our devices is believed to be due primarily to the increased 1D subband spacings relative to the magnitude of potential fluctuations in the channel region. Our explanation is shown to be in agreement with recent theoretical analyses relating various scattering mechanisms to the breakdown of quantized conductance. [S0163-1829(96)03719-8]

I. INTRODUCTION

The phenomenon of quantized conductance has been a topic of great interest since its initial observation in split-gate ballistic constrictions (or quantum point contacts) several years ago.[1,2] The conductance G of a constriction with arbitrary dimensions at zero temperature is given by the Landauer-Buttiker[3,4] formula

$$G=\frac{2e^2}{h}\sum_{i,j}^{n} T_{ij}, \tag{1}$$

where e is the electron charge, h is Planck's constant, n is the number of occupied one-dimensional (1D) subbands, and T_{ij} is the transmission probability for an electron incident in subband i exiting the constriction in subband j. Even though none of the constriction properties such as width, length, or subband energies appear explicitly in (1), a great deal of information is contained in the transmission factor T_{ij}. For the conductance to be quantized, the summation of the probabilities in (1) should approach the number of occupied subbands n. In point-contact geometries where the lithographic length L of the channel is less than $\sim$ 0.2 μm, electrons typically propagate through the constriction without scattering, i.e., ballistically. In this case, T_{ij} can be replaced by δ_{ij}, where the latter term is the Kronecker delta function. The summation in (1) then equals n and the conductance is quantized at values of $G=2ne^2/h$. It is important to note that though ballistic transport is sufficient for the observation of quantized conductance, it is not a necessary condition. Forward scattering between 1D subbands does *not* alter the summation in (1); only backscattering events destroy the quantized conductance.[5,6] Because ballistic constrictions are essentially quasi-1D, it might be expected that backscattering would be suppressed compared to the 2D case, due to the large momentum transfer required for these processes in a 1D system.[7] From this, it might also be expected that the quantized conductance should persist in constrictions as long as or longer than the 2D transport mean free path $l_{\rm tr}=\hbar k_F \mu_e/e$, where k_F is the Fermi wave vector and μ_e is the electron mobility. Therefore, it was somewhat unexpected when Timp *et al.*[8] found that the quantized conductance deteriorated significantly in constrictions with lithographic channel lengths greater than $\sim$ 0.6 μm, even in very high quality molecular-beam epitaxy (MBE) grown samples where $l_{\rm tr}$ exceeded 9 μm.[9] Timp *et al.* also noted that the quality of the quantized conductance in constrictions of various lengths was highly dependent upon the transport properties of the two-dimensional electron gas (2DEG).[10] They found that the quantized conductance for a given length constriction deteriorated as the mean free path of the 2DEG was reduced.

Since the initial observations of Timp *et al.*, several theoretical explanations for the breakdown of quantized conductance in longer constrictions have emerged.[6,11–14] These analyses attribute the degradation of quantized conductance to potential fluctuations caused by the random distribution of remote impurities. Numerical simulations of GaAs/Al_xGa_{1-x}As heterostructures have revealed a correlation length of $\sim$ 0.2 μm for the potential fluctuations.[11] These simulations have led some researchers to set an upper length of $\sim$ 0.5 μm for the observation of quantized conductance,[11] in agreement with the experimental results of Timp *et al.* However, reports in the literature have shown that quantized conductance can be observed to much greater lengths.[15,16] Most notably, Ismail, Washburn, and Lee[15] re-

ported the observation of quantized conductance steps in constrictions with channel lengths as long as 2 μm. These constrictions were not fabricated using the split-gate method, but rather by a low-damage deep-etching technique. In addition, Snider[17] found length-dependent results similar to those of Timp *et al.*, i.e., degradation of the quantized conductance for $L \gtrsim 0.6$ μm, but Snider's analysis was performed on a sample with a value of l_{tr} about one-fifth that of Timp *et al.*

In this paper we report on the length dependence of quantized conductance in split-gate constrictions fabricated on InAs quantum wells clad on either side by AlSb barrier layers. These studies may help develop a more comprehensive understanding of the lengths at which breakdown of quantized conductance occurs. Ballistic constrictions fabricated on InAs/AlSb materials may also have potential for observation of quantized conductance at increased lengths compared to GaAs/Al_xGa_{1-x}As. The remainder of this paper describes our detailed length-dependent experiments on InAs-channel ballistic constrictions. In Sec. II we give a motivation for using InAs/AlSb quantum wells for the realization of ballistic constrictions. Section III describes the experimental details and explains some of the properties of InAs/AlSb split-gate devices that are important when performing measurements and analyzing the subsequent data. Section IV details our length-dependent results and indicates considerably different length-dependent behavior than previous studies on GaAs/Al_xGa_{1-x}As. We also discuss the relative sensitivity of devices with various lengths to the impurity configuration in the vicinity of the 1D channel. The 1D subband spacings of a 2.0-μm-long device are quantitatively determined using temperature-dependent measurements. In Sec. V we compare our experimental results to the various theoretical predictions. We show that the length dependence of quantized conductance in InAs/AlSb constrictions approaches the theoretical limits set by first-order scattering models. We further argue that higher-order scattering processes are suppressed in our devices due to the energy spacing of the 1D subbands exceeding the magnitude of impurity potential fluctuations. This explanation is shown to be consistent with previous experimental studies and recent theoretical predictions concerning scattering via quasilocalized states in 1D constrictions. Finally, our conclusions are presented in Sec. VI.

II. MOTIVATION

The InAs/AlSb material system has several distinct differences from the more commonly studied GaAs/Al_xGa_{1-x}As material system. First, the effective mass of InAs ($m_\Gamma^* = 0.023m_0$) is approximately one-third that of GaAs. Therefore, the energy spacing of the 1D subbands in InAs should be considerably larger than those for GaAs. For nominally identical lateral potential profiles, as depicted in Fig. 1(a), one would expect a subband spacing ratio of $\Delta E_{1D}(\text{InAs})/\Delta E_{1D}(\text{GaAs}) \approx 1.5$–$2.5$. Such a direct comparison of 1D structures has not been performed as far as we know; therefore, the actual advantage gained by using InAs is still undetermined. Nevertheless, previous studies on InAs/AlSb constrictions[18] have revealed 1D subband spacings up to 12 meV, which are considerably larger than most GaAs/Al_xGa_{1-x}As split gates reported in the literature. An-

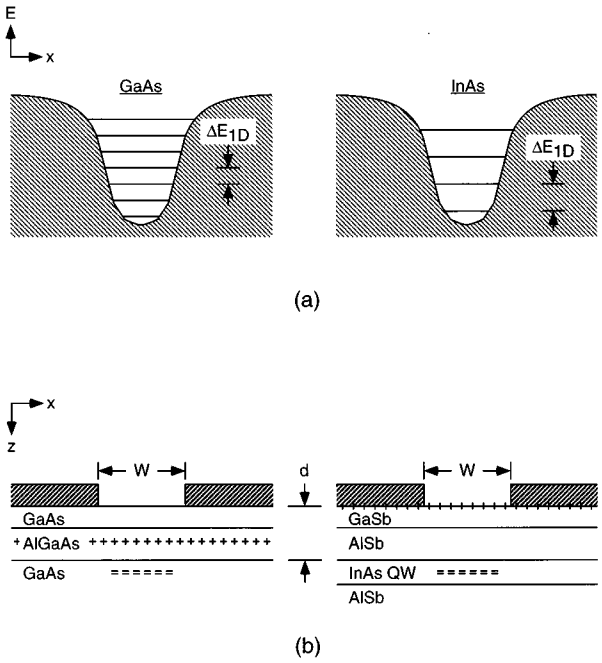

FIG. 1. (a) Illustration of lateral potential profile produced by split-gate confinement for GaAs and InAs channels. For identical confining potentials, the energy spacing of the 1D subbands should be considerably larger in InAs than in GaAs. (b) Schematic cross-sectional diagram of split-gate structures on InAs/AlSb and GaAs/Al_xGa_{1-x}As heterostuctures. The + symbols indicate the location of the primary doping layers in the two heterostructures.

other intriguing feature of InAs/AlSb quantum wells is their unique doping mechanism.[19–23] Large electron concentrations can be obtained in InAs/AlSb quantum wells without the addition of intentional dopants.[24] Figure 1(b) shows cross-sectional diagrams of split-gate devices fabricated on GaAs/Al_xGa_{1-x}As and InAs/AlSb 2DEG heterostructures. A 2DEG is typically obtained at the GaAs/Al_xGa_{1-x}As heterointerface by inserting a δ-doping layer into the top Al_xGa_{1-x}As barrier layer. Though this modulation-doping scheme is responsible for the very high mobilities achieved in these structures, scattering from potential fluctuations caused by the remote dopants dominates the transport properties, especially in near-surface 2D layers. As indicated schematically in Fig. 1(b) electrons in InAs/AlSb quantum wells originate from donors located at the surface of the GaSb capping layer.[19] Therefore, scattering from remote impurities should be reduced in InAs/AlSb due to the absence of a nearby doping layer.

Practically all of the previous experimental studies on ballistic constrictions have utilized the GaAs/Al_xGa_{1-x}As material system. The properties listed above make InAs/AlSb quantum wells an attractive alternative for studying the length dependence of 1D ballistic transport because they may allow the study of this complex problem in a parameter space different from GaAs/Al_xGa_{1-x}As. For instance, to increase ΔE_{1D} in a typical split-gate device, the spacing between the 2DEG and the surface d needs to be decreased. In GaAs/Al_xGa_{1-x}As this requires the thickness of the spacer layer between the δ-doping layer and the 2DEG to also be decreased. Therefore, an increased value of ΔE_{1D} is accom-

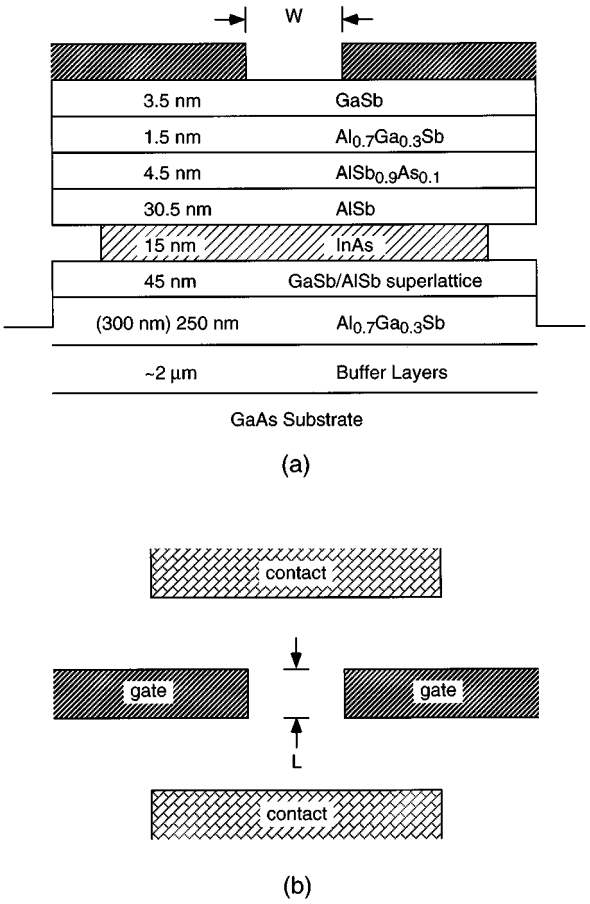

FIG. 2. (a) Cross-sectional diagram of device structure, showing the epitaxial layers of the InAs/AlSb heterostructure used in the present experiment. A selective wet chemical etch is used to undercut the InAs quantum well to avoid shorting to the gate electrodes. Values inside parentheses indicate where the layer thicknesses in wafer *B* differ from wafer *A*. (b) Schematic top view of general split-gate device configuration.

panied by a corresponding decrease in electron mobility and very likely an increase in potential fluctuations from the remote impurities. However, for the reasons listed above, InAs/AlSb split-gate constrictions should make possible a different regime, more difficult to obtain in $GaAs/Al_xGa_{1-x}As$, where the subband spacings are larger than the random potential variations. Therefore, our studies of quantized conductance in InAs/AlSb constrictions should help elucidate the relative importance of various constriction parameters on quantized conductance. Such studies may also clarify the apparent discrepancies in the literature concerning the length dependence of quantized conductance, as well as help determine some of the ultimate capabilities of ballistic constrictions.

III. EXPERIMENT

The experiments were performed on epitaxial layers grown by MBE. Two nearly identical layer structures were grown, which are labeled wafers *A* and *B*; growth details for wafer *A* are described elsewhere.[18] A schematic cross section of the layers for wafer *A* are shown in Fig. 2(a). Parentheses

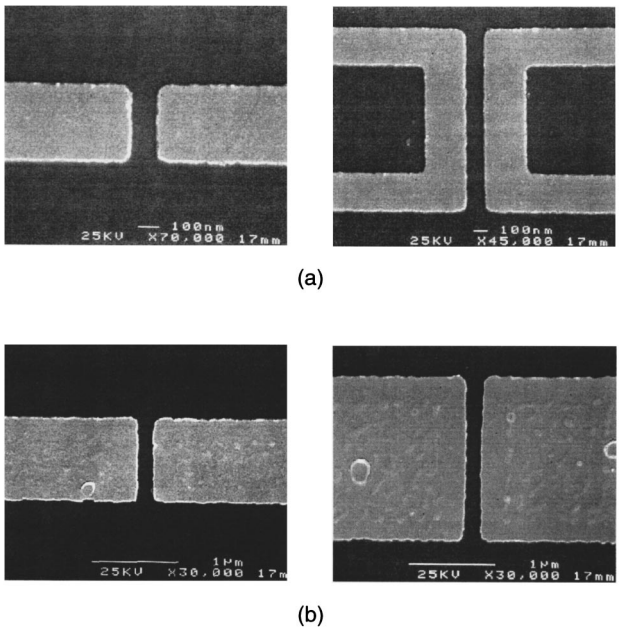

FIG. 3. Scanning electron micrographs (SEMs) of various split-gate geometries on (a) wafer *A* and (b) wafer *B*. The gates in (a) have $L=0.4$ and 1.5 μm and were patterned by electron-beam lithography using 50-kV electrons. The gates in (b) have $L=1.0$ and 2.0 μm and were patterned with an accelerating voltage of 25 kV.

indicate where the thickness of layers differed in wafer *B*. The electron sheet concentration and mobility at 10 K were $n_s=6.5\times10^{11}$ cm^{-2} and $\mu_e=3.8\times10^5$ cm^2/V s for wafer *A* and $n_s=4.5\times10^{11}$ cm^{-2} and $\mu_e=3.4\times10^5$ cm^2/V s for wafer *B*. These numbers lead to transport mean free paths of $l_{tr}=5.1$ and 3.8 μm, respectively. The constrictions were fabricated by standard mesa etching and Cr/Au nonalloyed Ohmic contacts. The InAs quantum well was undercut using selective wet etching to avoid shorting of the quantum well to the gate electrodes. Figure 2(b) shows a top view of the general device configuration. The gates were patterned by electron-beam lithography using a rectangular split-gate geometry. Figure 3 shows electron micrographs of typical devices fabricated on wafers *A* and *B*. Different electron-beam writing equipment was used for patterning the gates on the different wafers, which accounts for the somewhat different shape of the constrictions in Figs. 3(a) and 3(b). The conductance was measured in either a two-point or a four-point configuration. For two-point measurements, a small ac bias of $V_{ds}\approx 100$–200 μV_{rms} was applied between source and drain contacts, while the ac source current I_s was monitored using a lock-in amplifier. For four-point measurements the same procedure was followed, except the voltage across the constriction V_c was measured using leads located 35 μm apart on either side of the constriction. In both the two- and four-point cases the series resistance R_s, was subtracted to determine the actual conductance of the constriction. Unless otherwise noted, the measurement temperature was 4.2 K.

InAs/AlSb ballistic constrictions exhibit two particular characteristics that are important to the interpretation of the conductance data. First of all, a finite conductance exists after the pinch off of the last subband. This conductance is believed to be associated with electron transport at the mesa edge, where the Fermi level is pinned in the conduction band

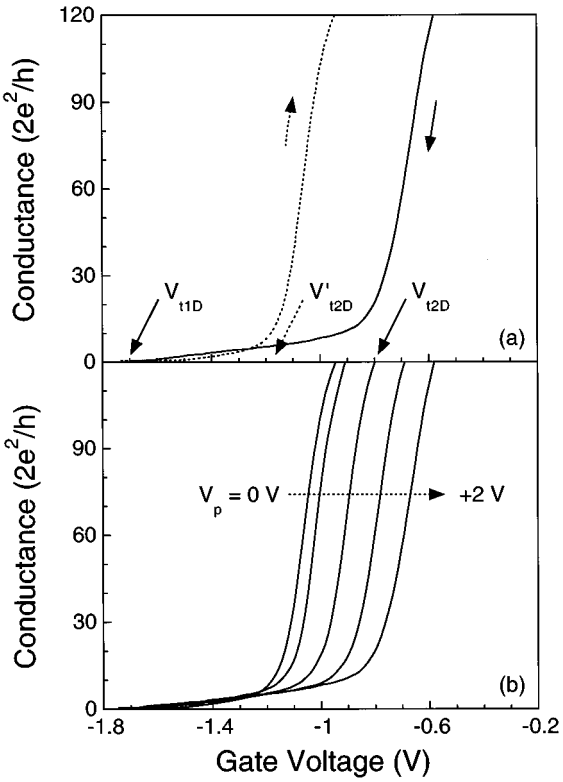

FIG. 4. (a) Conductance vs gate voltage trace for a typical ballistic constriction device. The solid (dashed) line shows the characteristic for the down sweep (up sweep). The 2D threshold voltage of the up sweep, V'_{t2D} is shifted negatively with respect to the threshold on the down sweep, V_{t2D}. Ensuing measurements between $V_g=0$ and V_{t1D} generally follow the dashed line, in both sweep directions. The voltage at which the 1D region is depleted V_{t1D} typically remains roughly constant. (b) Conductance data after application of different positive gate voltages before each measurement; larger positive voltages shift V_{t2D} to the right. All data are taken as a function of decreasing gate-source bias. The measurement temperature is $T=4.2$ K.

of InAs.[25] The magnitude of the parallel conductance $G_{\|}$ varies somewhat from device to device, usually within the range of 20–70 μS. Because $G_{\|}$ is essentially constant as a function of gate voltage, it is normally subtracted out to obtain the true conductance of the constriction. Using this procedure, the total normalized conductance G_n for two-point measurements can be determined as

$$G_n=\frac{1}{(V_{ds}/I_s-R_s)}-G_{\|}. \tag{2}$$

For four-point measurements, the constriction voltage V_c, replaces V_{ds} in (2). Except where noted, the normalized conductance G_n as determined by (2) is presented in this paper.

Second, we have found that, for all devices tested, the conductance characteristic is dependent upon the sweep direction and the bias history of the gate voltage.[26] The term ''bias history'' means whether or not a large positive or negative voltage has most recently been applied to the gates. Figure 4 shows a typical (unnormalized) conductance vs gate voltage trace for an InAs/AlSb split-gate device. As the gate bias, V_g is swept toward more-negative values, the 2D regions underneath the gates are depleted at $V_g=V_{t2D}$ and the fringing fields from the gates eventually pinch off the 1D channel at $V_g=V_{t1D}$. If V_g is swept back toward zero from its most negative point, as indicated by the dashed line in the figure, we find that V_{t2D} shifts negatively. Subsequent up and down sweeps between $V_g=0$ and V_{t1D} tend to follow the dashed line in the figure, thus obscuring any quantized conductance characteristic that may have been observed on the initial down sweep. We have found that V_{t2D} can be shifted back toward its original value by applying a positive voltage to the gate electrodes before each measurement. After application of this positive premeasurement bias voltage V_p, V_{t2D} shifts back toward more-positive values [Fig. 4(b)]; the larger the value of V_p, the more positive the shift in V_{t2D}. The ensuing up sweep always shows the hysteresis observed on the initial trace. The threshold at which the constriction pinches off, V_{t1D}, typically is not altered by V_p.

We believe the dependence of the constriction characteristics on the bias history of the gates is due to the charging (or discharging) of impurity or surface states underneath the gate electrodes. After the application of a large negative (positive) gate bias, the states remain charged until a large bias of the opposite sign is applied to gates. For a given premeasurement bias voltage, the ensuing down sweep is extremely repeatable and indicates that the amount of charge accumulated under the gates is consistent for a particular value of V_p. We will discuss later our belief that V_p also affects the *configuration* of ionized impurities in the vicinity of the 1D channel. For the present length-dependent analysis, the premeasurement bias voltage is used primarily as a method of obtaining consistent conductance vs gate voltage traces. Unless otherwise indicated, a voltage of $V_p=+2.0$ V has been applied to the gates for 1–2 min before each measurement. A rather large value of V_p is chosen in order to increase $V_{t2D}-V_{t1D}$ and therefore more effectively probe the constriction characteristics. In addition, all data are taken as a function of decreasing gate-to-source voltage only.

IV. RESULTS

A. Length dependence

Constrictions with channel lengths varying from 0.20 to 2.0 μm were fabricated on both wafers *A* and *B*. The lithographic width of the devices fabricated on *A* varied from 0.12 μm in the shortest constrictions to 0.16 μm for the longest devices. The width of constrictions on wafer *B* were approximately 0.05 μm wider than those for *A* due to the lower electron concentration in wafer *B*. Quantized conductance characteristics for constrictions patterned on the higher-mobility material are shown in Fig. 5. The data in this figure and in Fig. 6 represent the ''best'' devices for each length used in this study. Here the term ''best'' refers to devices whose quantized conductance values are closest to the ideal values of $2ne^2/h$. Ideally, as part of a quantitative length-dependent study, it would be desirable to perform a statistical analysis of the quantization for each length due to the varying nature of the device parameters and changing impurity configuration from device to device. Unfortunately, the number of devices at each length that would need to be tested to perform a meaningful statistical analysis is beyond our means at the present time. However, subsequent figures

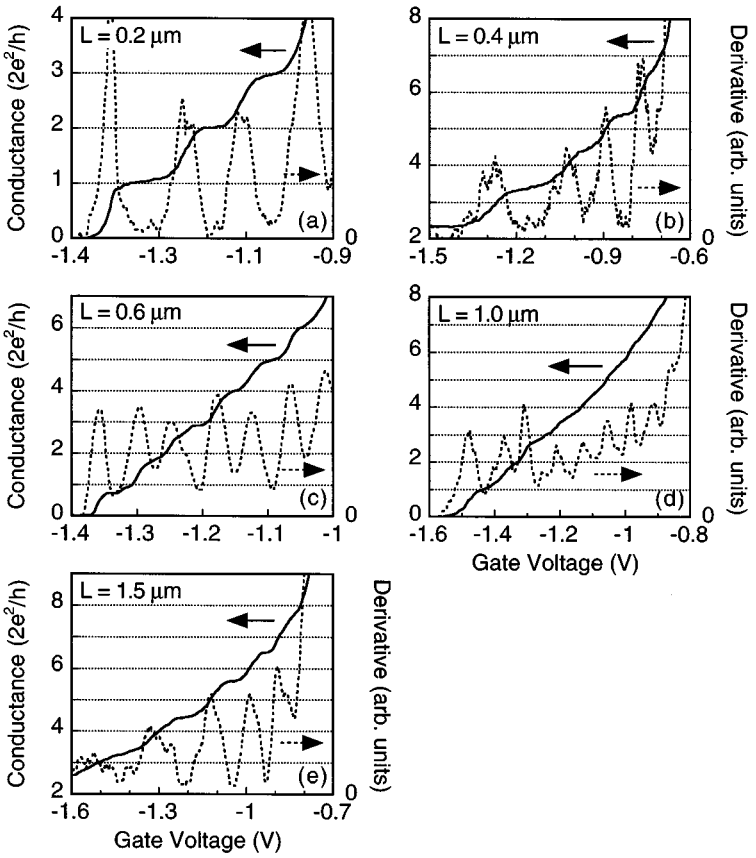

FIG. 5. Quantized conductance characteristics for constrictions patterned on wafer *A* with lithographic channel lengths of (a) 0.2 μm, (b) 0.4 μm, (c) 0.6 μm, (d) 1.0 μm, and (e) 1.5 μm. The constriction conductance is indicated by the solid line, while the derivative of the mathematically smoothed conductance data is shown by the dashed line. The measurement temperature is $T=4.2$ K.

do give an indication of the types of variations that occur for different device lengths. Figure 5 shows quantized conductance traces for constrictions of width $L=0.2$, 0.4, 0.6, 1.0, and 1.5 μm. The constrictions with $L=0.4$ and 1.5 μm could not be pinched off before the onset of excessive gate-leakage current. Because of this, the parallel conductance could not be determined and therefore was not subtracted when normalizing the data. Despite variations in the sharpness of the steps for the different lengths, each device shows conductance steps with spacing approximately equal to $2e^2/h$. Eight well-quantized conductance steps are observed in the $L=1.0$ μm constriction, while at $L=1.5$ μm five conductance steps are observable.

Constrictions with various lengths were also fabricated on wafer *B*, which had a value of $l_{\rm tr}$ approximately 25% less than that for wafer *A*. The results of these measurements are shown in Fig. 6. Once again, quantized conductance is observed for all three device lengths. As expected, the step spacings of the shortest device with $L=0.6$ μm are closest to the ideal values of $2e^2/h$. Nonidealities in the quantization begin to appear for $L=1.0$ μm [Fig. 6(b)], where the heights of the low-index steps are considerably nonideal, but the step spacing improves for higher n. Surprisingly, in Fig. 6(c) at $L=2.0$ μm, the quantization is better than that for the 1.0-μm constriction. Some deviations from ideality occur, but they are not as severe as in the 1.0-μm-long device. The data of Fig. 6(c) indicate that quantized conductance can persist in constrictions with lengths over 50% of the 2D mean free path. Our results are in noticeable contrast to those of Timp *et al.*,[8] where the quantized conductance deteriorated dramatically at constriction lengths $<10\%$ of the 2D mean free path. In that study, 0.2-μm-long constrictions fabricated on GaAs/Al_xGa_{1-x}As 2DEG's with $l_{\rm tr}\approx 10$ μm showed extremely well quantized steps, while constrictions with $L=0.6$ μm fabricated on the same material had severely degraded characteristics. In Snider's length-dependent analysis,[17] performed on a GaAs/Al_xGa_{1-x}As heterostructure with $l_{\rm tr}=2.1$ μm, the quantized conductance was rapidly destroyed with increasing length, with remnants of the fundamental plateau persisting to $L\approx 0.6$ μm.

It is useful to compare the actual quantization values for constrictions of different lengths. The quantization for each step Q_n is determined as

$$Q_n=\frac{G(n)h}{2ne^2}, \tag{3}$$

where $G(n)$ is the conductance step height, defined as the value of the conductance that corresponds to a minimum in the mathematical derivative (shown in Figs. 5 and 6). The average quantization $Q_{\rm av}$ is then determined by averaging over all clearly observable steps N,

$$Q_{\rm av}=\frac{1}{N}\sum_{n=1}^{N} Q_n. \tag{4}$$

The quantization is defined in this manner because the quantization values obtained give an indication of the transmission probability through the constriction, even if the conductance characteristic is smeared by temperature, bias voltage, or parasitic effects such as heating from gate leakage. In this way, if the transport is ballistic, even at finite temperatures

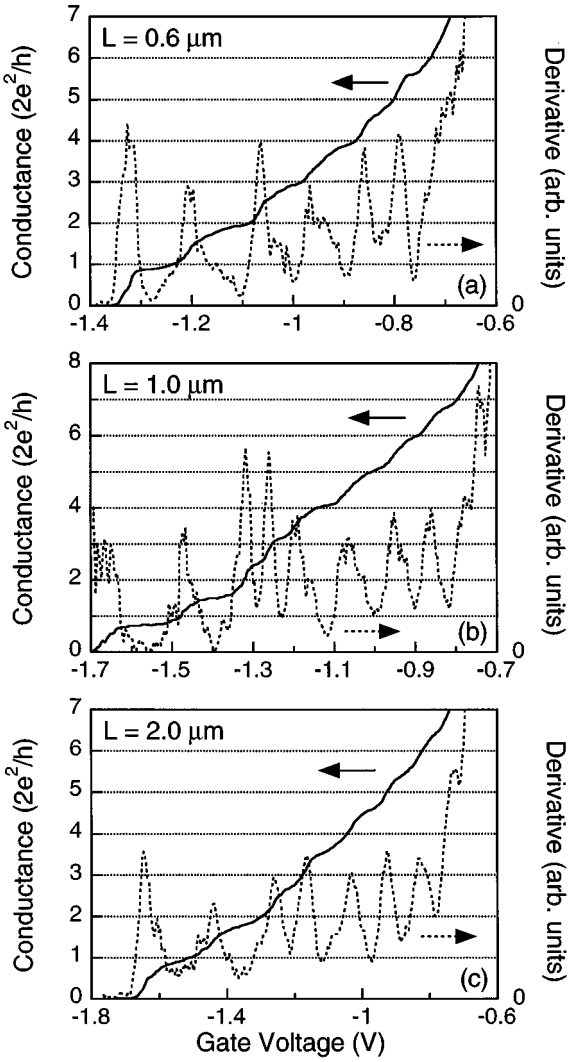

FIG. 6. Quantized conductance characteristics for constrictions patterned on wafer *B* with lithographic channel lengths of (a) 0.6 μm, (b) 1.0 μm, and (c) 2.0 μm. The constriction conductance is indicated by the solid line, while the derivative of the mathematically smoothed conductance data is shown by the dashed line. The measurement temperature is $T=4.2$ K.

and bias voltages, the conductance step heights should be equal to $2ne^2/h$, and from (3) and (4), $Q_n=Q_{\mathrm{av}}=1$, for all n. The error values quoted in this paper indicate the uncertainty in determining the precise value of conductance associated with a minimum in the mathematical derivative. Table I shows a comparison of Q_{av} for devices with $L=0.2$ and 1.0 μm fabricated on wafer *A* and $L=0.6$, 1.0, and 2.0 μm on *B*. The quantized conductance characteristics of these devices are shown in Figs. 5(a) and 5(d) and Figs. 6(a)–6(c), respectively. Despite the fact that the conductance steps for $L=1.0$ μm are somewhat smeared out, $Q_{\mathrm{av}}=0.96\pm0.08$. The deviation from ideality is small and shows little degradation compared to the 0.2-μm-long device, where $Q_{\mathrm{av}}=1.02\pm0.04$. The constrictions with $L=0.4$ and 1.5 μm shown in Figs. 5(b) and 5(e), respectively, also have nearly ideal quantization. However, because the parallel conductance could not be determined, it is difficult to extract the quantization values from the experimental data. Furthermore, it should be noted

TABLE I. Average quantization values of constrictions with conductance characteristics shown in Figs. 5 and 6. The quantization value for a given step Q_n, where n is the subband index, is determined as the value of the normalized conductance that corresponds to the minimum of the mathematically determined $\partial G_n/\partial V_g$ vs V_g curve. The average quantization Q_{av} is determined by averaging the values of Q_n for all clearly observable steps. Ideal quantization would correspond to a value of $Q_{\mathrm{av}}=1$.

Wafer	l_{tr} (μm)	L (μm)	No. of steps	Q_{av}
A	5.1	0.2	3	1.02 ± 0.04
A	5.1	1.0	8	0.96 ± 0.08
B	3.8	0.6	6	0.93 ± 0.05
B	3.8	1.0	8	0.80 ± 0.11
B	3.8	2.0	7	0.89 ± 0.05

that since the lower-index steps of the 1.5-μm-long device could not be probed, nonideal quantization may exist for these steps. For the devices fabricated on wafer *B*, Table I clearly shows that the quantization is best for the $L=0.6$ μm constriction, deteriorates at $L=1.0$ μm, and then surprisingly improves for $L=2.0$ μm. For the $L=2.0$ μm device shown in Fig. 6(c), Q_{av} is within $\sim$10% of the ideal values and the step heights at this length are only slightly lower than those for $L=0.6$ μm.

B. Effect of impurities

Despite the fact that quantized conductance can be observed in constrictions as long as 2.0 μm, longer devices appear to be more sensitive to the precise impurity configuration than short devices. First of all, longer constrictions tend to show greater variations between nominally identical devices than shorter devices. To illustrate this property, Fig. 7(a) shows three nominally identical 0.2-μm-long constrictions fabricated on wafer *A*. Clearly, the sharpness of the conductance steps varies considerably from device to device, but the heights of the conductance plateaus do not deviate a great deal from the ideal values of $2ne^2/h$. The device variations become more pronounced when the device length is increased to 1.0 μm however. Figure 7(b) shows three constrictions with $L=1.0$ μm (two fabricated on wafer *A* and one on wafer *B*). At this length, significant deviations from ideal quantization are observed, as well as variations in the sharpness of the steps. For devices with $L=2.0$ μm, some form of quantized conductance is evident in each device; however, both the heights and sharpness of the steps vary considerably from device to device. The two rightmost characteristics in Fig. 7(c) have very nonideal quantization, in some cases with step heights less than half of the ideal values of $2ne^2/h$. However, the device corresponding to the leftmost trace in Fig. 7(c) has quantized step heights much closer to $2ne^2/h$ than the other devices with $L=2.0$ μm. The large variations that occur in nominally identical constrictions make it easier to understand the somewhat anomalous quantization values in Table I. Presumably, the somewhat poorer quantization in the device with $L=1.0$ μm, compared to the best 2.0-μm constriction, can be explained as being within the normal expected range of statistical variations for long devices.

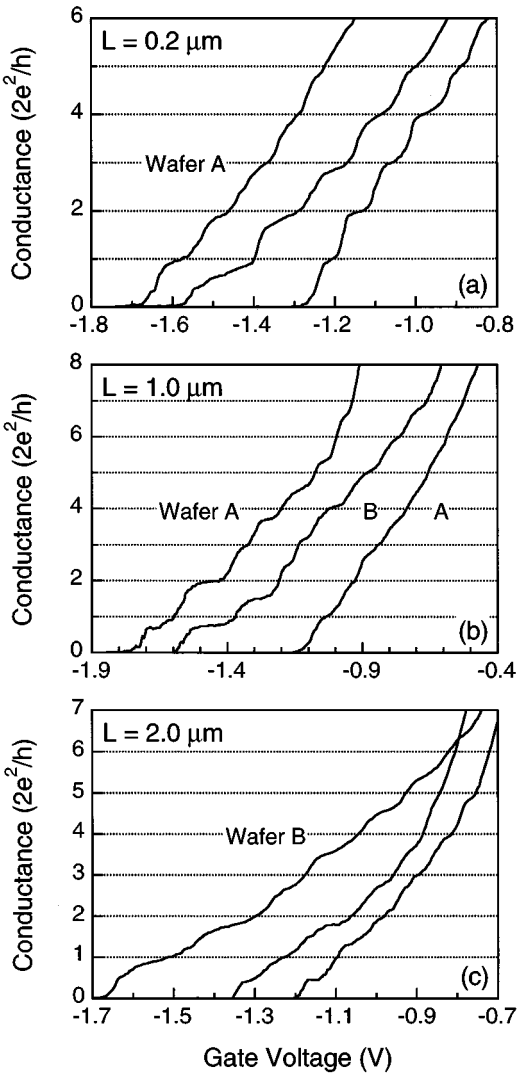

FIG. 7. Conductance data taken at $T=4.2$ K for three sets of constrictions with lithographic channel lengths of (a) 0.2 μm, (b) 1.0 μm, and (c) 2.0 μm. In each case, the curves have been shifted along the voltage axis for purposes of clarity. (a) For $L=0.2$ μm, despite variations in the sharpness of the quantized conductance, step heights very close to $2ne^2/h$ are typically observed. (b) For $L=1.0$ μm, more significant variations from ideal values can occur, though sharp conductance steps and nearly ideal quantization can be observed. (c) The device variations are most severe in the longest constrictions with $L=2.0$ μm. Here very nonideal quantization is observed in two devices, particularly for the low index steps $n=1$–3. However, the quantized conductance of a third constriction shows much more ideal step spacing.

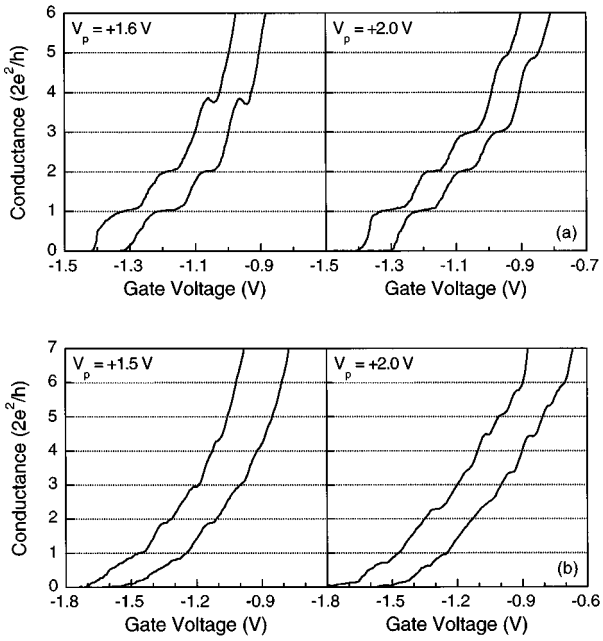

FIG. 8. Variations of the conductance characteristics as a function of premeasurement bias voltage V_p, explained in Sec. III. (a) Conductance vs gate voltage of a short constriction ($L=0.2$ μm) for a voltage of $V_p=+1.6$ and $+2.0$ V applied before measurement. Two consecutive sweeps at this voltage are shown displaced by 0.1 V. Data at each value of V_p are repeatable, while nonidealities in the quantization differ as V_p is changed. (b) Conductance characteristic of a $L=1.0$ μm constriction [different from the device shown in Fig. 5(f)] for $V_p=+1.5$ and $+2.0$ V. The quantized conductance is weakened compared to (a). However, steps are still visible for $V_p=+1.5$ V, while at $V_p=+2.0$ V quantization is almost completely obscured. The measurements for the same value of V_p at $L=1.0$ μm are also not as repeatable as in the shorter device. The measurement temperature is $T=4.2$ K.

We stated in Sec. III that the application of a positive premeasurement bias voltage V_p can reproducibly shift the 2D threshold voltage V_{t2D}. Since this effect is attributed to the charging and/or discharging of impurities or surface states, one would also expect that the additional charges would affect the quantized conductance as well. In Fig. 8(a) the conductance characteristic of a short constriction ($L=0.20$ μm, $W=0.10$ μm) is shown for different values of V_p. The signature of an isolated impurity is evident in the characteristic corresponding to $V_p=+1.6$ V and is consistent after repeated measurements, as indicated in the figure. This behavior indicates that the position of the impurity with respect to the 1D channel is the same for a given value of V_p. However, the characteristic changes somewhat when V_p is increased to $+2.0$ V. The differences in the plots for $V_p=+1.0$ and $+2.0$ V suggest that different premeasurement voltages may slightly alter the impurity configuration with respect to the position of 1D channel. Figure 8(b) shows the V_p dependence of a $L=1.0$ μm constriction. Clearly, the characteristic at $V_p=+1.5$ V is considerably different than the one for $V_p=+2.0$ V. In fact, whereas quantized conductance is observable for $V_p=+1.5$ V, the steps are considerably obscured for the latter case. Though slight differences typically occur for shorter devices, as in Fig. 8(a), it is not uncommon for a long device to undergo wide variations for different values of V_p. This behavior indicates that long constrictions are more sensitive to slight changes in the impurity configuration than shorter ones. Figure 8(b) also illustrates that consecutive traces for a given value of V_p are not as reproducible for $L=1.0$ μm as for $L=0.2$ μm. This would suggest that the configuration of impurities with respect to the 1D channel is not exactly reproduced for a given value of V_p, as the length of the constriction is increased. A final indication of the effect of impurities on the constriction characteristics is their sensitivity to temperature cycling. Raising and then lowering the temperature of split gates fabricated on

$GaAs/Al_xGa_{1-x}As$ material has previously been shown to change the distribution of ionized impurities.[10,27] Both devices in Fig. 8 were cycled from 4.2 to ~160 K and then back to 4.2 K. While the short device retained its characteristic almost exactly, the 1.0-μm split-gate characteristic was altered considerably.

Another factor that may cause wide variations between long devices with similar geometries (as in Fig. 7) is residual impurities in the InAs quantum well. An ionized impurity directly in the InAs layer will likely act as an isotropic scattering center and could have a significant effect on the electron transport through the constriction. For a reasonable background concentration of $N_b=10^{15}$ cm^{-3}, we would expect ~3 of these impurities in a constriction with dimensions $W=0.1$ μm and $L=2.0$ μm. A change in the number of actual impurities from device to device combined with variations in their precise location could likely cause the wide conductance variations observed in our devices. These variations are expected to be enhanced as the constriction length is increased due to the increased number of impurities probed by longer constrictions. Fortunately, unlike the intentionally introduced dopants in $GaAs/Al_xGa_{1-x}As$ heterostructures—a necessary part of the device characteristics—the background impurity concentration in our heterostructures should be reduced as the MBE growth technology is improved.

C. Determination of subband spacings

To understand the possible correlation between subband splittings and enhanced length-dependent behavior in InAs-channel constrictions, we have performed temperature-dependent measurements on the 2.0-μm-long constriction whose characteristic is shown in Fig. 6(c). For this study, a direct analog measurement of the differential conductance is taken. A dc bias of $V_{ds}=1$ mV is applied between source and drain contacts, while a small 19 Hz sinusoidal voltage of 10 mV_{rms} is placed in series with the ramp voltage applied to the gates. The ac component of the source current is monitored using a lock-in amplifier. In this configuration the detected signal is proportional to the (unnormalized) differential conductance $\partial G/\partial V_g$. As shown in Fig. 9(a), the differential conductance at low temperatures is an oscillatory function of the gate voltage. Figures 9(b)–9(d) show the effect of temperature on the differential conductance oscillations for the $L=2.0$ μm device. Remnants of the conductance oscillations persist to about $T=35$ K. We quantitatively determine the 1D subband spacings, ΔE_{1D} by analyzing the temperature dependence of $\partial G/\partial V_g$ using a method similar to Refs. 28 and 29. To perform this analysis, we define the values $d_{max}=\partial G/\partial V_g|_{max}$ and $d_{min}=\partial G/\partial V_g|_{min}$ that correspond to the maximum and minimum of the differential conductance for each 1D subband, respectively. The quantity $(d_{max}-d_{min})/(d_{max}+d_{min})$ is then plotted as a function of temperature for each subband and compared with theory. Figure 10 shows the temperature dependence of the ratio $(d_{max}-d_{min})/(d_{max}+d_{min})$ for steps corresponding to $n=1$ and 4.

For the theoretical analysis we start by assuming a drain-source voltage that approaches zero and $T_{ij}=\delta_{ij}$, where δ_{ij} is the Kronecker delta function. The former assumption is justified since the 1-mV drain-to-source voltage is much smaller than the 1D subband spacings. The latter relation basically assumes ballistic transport through the constriction, which is a reasonable assumption given the good quality of the quantized conductance for this device. Reflections due to the gate geometry, scattering from impurities, heating from gate leakage, or any other effects that tend to smear the steps are not explicitly introduced, but are instead lumped into an effective temperature T_0. Using these assumptions the quantized conductance at finite temperature becomes

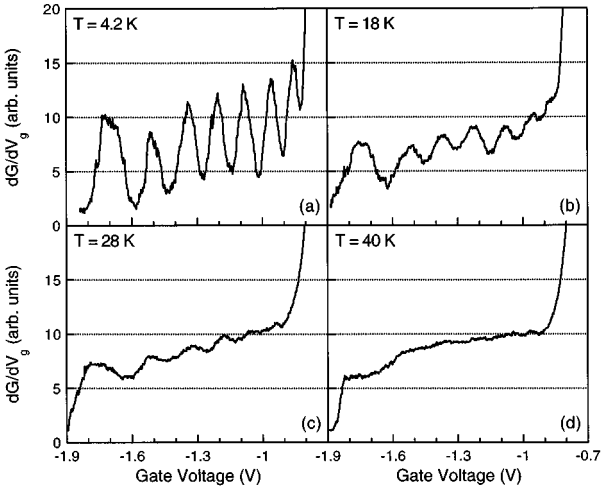

FIG. 9. Temperature dependence of the analog $\partial G/\partial V_g$ vs V_g curve for a $L=2.0$ μm constriction fabricated on wafer B. The G vs V_g characteristic of this device is shown in Fig. 6(c). Measurements at $T=4.2$, 18, 28, and 40 K are shown in (a)–(d), respectively. Oscillations in the differential conductance were observed to temperatures as high as 35 K.

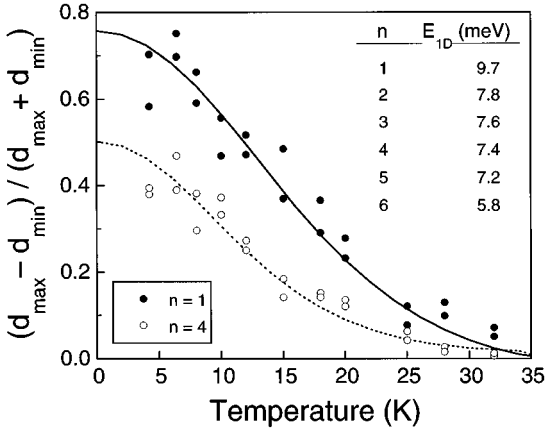

FIG. 10. Fit of experimental data in Fig. 9 to theoretical values computed using Eqs. (5)–(7). The maximum $d_{max}=\partial G/\partial V_g|_{max}$ and minimum $d_{min}=\partial G/\partial V_g|_{min}$ of the differential conductance are determined for each value of the subband index n. The ratio $(d_{max}-d_{min})/(d_{max}+d_{min})$ is plotted vs temperature for $n=1$ and 4. These data are indicated by the solid and open circles, respectively. The best-fit curves for $n=1$ and 4 are indicated by the solid and dashed lines, respectively. The best-fit values of the subband spacings ΔE_{1D} for each subband n are listed in the figure. The background temperature T_0 was held constant for all subbands; a value of $T_0=14$ K was found to fit the data most closely.

$$G_d=\frac{2e^2}{h}\sum_n \frac{1}{1+\exp[(E_n-E_F)/kT_{\rm eff}]}, \tag{5}$$

where

$$T_{\rm eff}=\sqrt{T^2+T_0^2}. \tag{6}$$

Finally, the effect of the series resistance is taken into account, so that the total calculated conductance becomes

$$G=\frac{1}{(1/G_d+R_s)}. \tag{7}$$

Using $\Delta E_{1D}=E_n-E_{n-1}$ and T_0 as adjustable parameters and assuming that E_F varies linearly with V_g, the conductance G is calculated as a function of V_g. The differential conductance $\partial G/\partial V_g$ is then calculated numerically and the theoretical values of $(d_{\max}-d_{\min})/(d_{\max}+d_{\min})$ are compared with experiment. The solid line in Fig. 10 represents the best fit of our numerical calculations to the experimental data for $n=1$ and 4. A value of $T_0=14$ K is found to fit the data most closely. The results of fits for the other subbands are shown in the inset. The subband spacings are seen to increase with decreasing gate voltage and vary from 5.8 meV for the highest lying subband to 9.7 meV for the fundamental mode in the constriction. These values are slightly lower than previous magnetic-field measurements on shorter constrictions fabricated on wafer A.[18] This discrepancy is expected due to the larger lithographic width used for devices fabricated on B. Our devices have much larger values of ΔE_{1D} than those of Timp *et al.* Simulations performed by Snider[17] revealed that those constrictions had $\Delta E_{1D}\approx 1.5$ meV. In the length analysis performed by Snider, subband spacings around 10 meV were reported. The deeply etched wire structure characterized by Ismail also had subband spacings around 10 meV.[30]

V. DISCUSSION

A comparison of our results with the previous theoretical work is useful in understanding the improved length performance observed in our devices. As stated in Sec. I, most of these theoretical studies have attributed the breakdown of the quantized conductance to scattering from potential fluctuations caused by remote impurities. Modulation doping of heterostructures such as $GaAs/Al_xGa_{1-x}As$ allows very large mobilities by spatially separating the dopants from the mobile charge carriers (typically electrons).[31] However, the dopants still produce random potential fluctuations in the conduction plane of the 2DEG.[32] Since the fluctuating potential profile is slowly varying on the scale of a Fermi wavelength, to first order, only small-angle scattering can occur. Glazman and Jonson[12] used the Born approximation to show that in a 1D constriction, small-angle scattering is suppressed *except* when a mode is newly populated. When a mode is just turned on, the momentum transfer required for backscattering is small. Therefore, such scattering events are likely to occur. However, backscattering in the lower-lying subbands is suppressed because of the large momentum transfer needed to reverse the direction of these electrons. Glazman and Jonson went on to show, for realistic constriction geometries, that small-angle scattering in the highest occupied mode is sufficient to obscure the quantized conductance.

Glazman and Jonson gave a criterion for the number of well-resolved steps n_q that should be observable in a 1D constriction in terms of the properties of the unconstrained 2DEG:

$$n_q \leqslant \frac{4.5}{\ln^2(2n_qL_0/l_s)}\frac{l}{l_s}, \tag{8}$$

where L_0 is the constriction length and $l_{\rm tr}$ and l_s are the transport and scattering mean free paths, respectively. For our wafer A we have $l_{\rm tr}=5.1$ μm and even though the value of l_s for our material is not known, a value of $l_{\rm tr}/l_s$ somewhere between 10–50 seems reasonable for fairly high quality 2DEG material.[33] Furthermore, we can estimate the actual channel length (rather than the lithographic length) as $L_0\approx L+W$, where L and W are the lithographic channel length and width, respectively. For our longest two devices fabricated on wafer A, we have $L_0=1.6$ and 1.1 μm. Inserting these values into (8), we obtain $n_q\leqslant 4$–8 and 5–8. For the longest constriction on B, we have $L_0=2.2$ μm and $l_{\rm tr}=3.8$ μm and thus obtain $n_q\leqslant 3$–6. These numbers are in reasonable agreement with the data in Figs. 5 and 6.

For comparison purposes we solved (8) for the devices of Timp *et al.*[8] and Snider.[17] For the former, $l_{\rm tr}=10.3$ and 9.5 μm, $L_0=0.9$ μm, and the same range of values for $l_{\rm tr}/l_s$ is assumed. Once again inserting these values into (8), we obtain $n_q\leqslant 7$–11 and 7–11. The number of clear conductance steps actually observed for those devices was $n_q\approx 3$ and 0. Similarly, in Snider's work, for $l_{\rm tr}=2.1$ μm and $L_0=0.7$ μm we obtain $n_q\leqslant 4$–7. The number of actual steps was $n_q\approx 1$. Clearly, (8) tends to be consistent with the our data on InAs constrictions, but significantly overestimates n_q for GaAs constrictions. One possible reason for this discrepancy is that additional mechanisms for backscattering may exist in $GaAs/Al_xGa_{1-x}As$ constrictions, beyond the first-order processes assumed by Glazman and Jonson. An increased backscattering probability would decrease the constriction length at which quantized conductance disappears or decrease the number of discernible steps for a given length. Glazman and Jonson's treatment also does not take into account the reduced sheet concentration of electrons in the 1D channel compared to the 2D regions. As noted previously,[34] the lower electron concentration reduces the screening of remote impurities that can lead to an increase in the fluctuation potential. For these reasons, we need to look beyond this first-order approach to understand the improved length-dependent behavior observed in InAs/AlSb constrictions.

Nixon, Davies, and Baranger[11] approached the problem of scattering in 1D wires in a different manner. They used numerical calculations to show that in constrictions longer than the correlation length of the potential fluctuations (~ 0.2 μm) quantized conductance can be seriously degraded. Laughton *et al.*[6] demonstrated that this impurity potential can create quasilocalized states in the channel, producing an indirect mechanism for electron backscattering. Scattering via quasilocalized states is not limited to the highest occupied 1D subband, but can occur for any propagating mode and becomes more probable with higher mode occupancy. This two-stage scattering mechanism was treated analytically by Zagoskin *et al.*,[14] who found that their analysis agreed favorably with numerical simulations similar to those of Nixon, Davies, and Baranger. More importantly, the analytical re-

sults of Zagoskin *et al.* showed that the density of quasilocalized states (that lead to the breakdown of quantized conductance) decrease exponentially with the ratio of the 1D subband spacings to the standard deviation of impurity potential fluctuations, $\Delta E_{1D}/\sigma_{imp}$.

The analyses of Laughton *et al.* and Zagoskin *et al.* take into account both screening and scattering mechanisms above simple first-order processes and therefore may be capable of explaining the contrasting length dependence between InAs/AlSb and GaAs/Al_xGa_{1-x}As constrictions. Unfortunately, the numerical studies are difficult to compare with experiment because they do not express the criterion for quantized conductance in terms of easily measurable quantities. However, the work of Zagoskin *et al.* establishes that an increased ratio of $\Delta E_{1D}/\sigma_{imp}$ can suppress scattering via quasilocalized states. The 1D subband spacings can readily be determined by temperature-dependent measurements, as we have shown in Sec. IV, and by magnetic-field measurements.[35] The term σ_{imp}, which is the standard deviation of the fluctuation potential, is not an easily determined quantity. However, Davies and Timp[36] determined a relation for σ_{imp} based upon simple electrostatics and a Thomas-Fermi screening model. Davies determined a value of $\sigma_{imp} \approx 1.6$ meV for the device structure used by Timp *et al.* The potential fluctuations are on the same order as the subband spacings ($\sim$1.5 meV) and should therefore produce a large number of quasilocalized states. For InAs/A1Sb quantum wells, the mobility is mainly limited by interface-roughness scattering and probably by residual impurities in the AlSb barrier layers and the InAs quantum well.[37] If the relation of Davies and Timp is used for our devices, the potential fluctuations arising from deep donors ($N_{DD}=10^{16}$ cm^{-3}) in the barrier layers on either side of the quantum well give $\sigma_{imp} \approx 2.4$ meV. We also estimate additional potential fluctuations of no more than 2 meV caused by nonuniformities in the InAs/AlSb interfaces.[38] The total standard deviation of the fluctuations would therefore be $\sim$3–4 meV, still less than our 1D subband spacings of 6–10 meV.

Our length-dependent data and subsequent comparison with theory give a strong indication that higher-order scattering mechanisms are suppressed in InAs/AlSb split-gate constrictions. This reasoning explains why the theoretical value of n_q is much larger than experiments actually indicate in GaAs, i.e., because scattering via quasilocalized states is neglected. Since $\Delta E_{1D}/\sigma_{imp}$ is small in GaAs split-gate devices, scattering from these states is expected to be important. In our devices, however, backscattering is suppressed, except in newly populated modes and therefore the theoretical value of n_q is in reasonable agreement with experiment. This reasoning could also explain the data of Ismail, Washburn, and Lee. Instead of using the split-gate method, they utilized a deep-etching technique that allowed them to fabricate devices with large subband spacings on very high mobility material, leading to a large $\Delta E_{1D}/\sigma_{imp}$ ratio, similar to our devices. Therefore, there appears to be no fundamental reason why large subband spacings cannot be obtained in GaAs without a substantial increase of the disorder in the wire region. Our studies do show, however, that InAs/AlSb quantum wells are better suited for this task than GaAs/Al_xGa_{1-x}As particularly when the split-gate configuration is used. For GaAs/Al_xGa_{1-x}As devices, one needs to find somewhat more clever methods of achieving large $\Delta E_{1D}/\sigma_{imp}$ ratios, thereby enhancing the length performance of 1D wires.

VI. SUMMARY

We have performed length-dependent analysis of quantized conductance in split-gate constrictions fabricated on InAs/AlSb quantum wells. Quantized conductance steps with heights within about 10% of $2ne^2/h$ are observed in constrictions as long as 2.0 μm. This length is over 50% of the 2D transport mean free path of 3.8 μm. The improved length dependence of our devices over GaAS/Al_xGa_{1-x}As split gates is shown to be in agreement with various theoretical analyses that describe the scattering mechanisms that lead to the breakdown of quantized conductance. One such mechanism is scattering via quasibound states in the 1D channel, the concentration of which is exponentially dependent upon the ratio of the 1D subband spacings to the standard deviation of potential fluctuations. By careful determination of the subband spacings in our devices and estimation of the potential fluctuations based upon existing theories, we show that large $\Delta E_{1D}/\sigma_{imp}$ ratios are likely realized in our devices. We further show that our length-dependent data approach the less stringent requirements set forth by the first-order scattering model used by Glazman and Jonson. Our studies do indicate, however, that longer constrictions ($L \gtrsim 1$ μm) are more sensitive to impurities in the vicinity of the 1D channel. This behavior is evidenced by an increased dependence on various experimental parameters such as the premeasurement bias voltage and temperature cycling. Continued improvement of the InAs/AlSb materials technology should allow further reduction of potential fluctuations caused by unintentional dopants and interface roughness. Additional studies are still needed to determine the precise length at which the quantized conductance can no longer be observed. Numerical simulations on InAs/AlSb heterostructures may also be useful in more accurately pinpointing the specific relation between the various constriction parameters and electron scattering in 1D constrictions.

ACKNOWLEDGMENTS

This work was support by the NSF Science and Technology Center for Quantized Electronic Structures, Grant No. DMR 91-20007, and was performed in part at the National Nanofabrication Facility, which is supported by the NSF under Grant No. ECS-8619049, Cornell University, and industrial affiliates.

*Permanent address: IBM Thomas J. Watson Research Center, P.O. Box 218, Yorktown Heights, NY 10598.

[1] B. J. van Wees, H. van Houten, C. W. J. Beenakker, J. G. Williamson, L. P. Kouwenhoven, D. van der Marel, and C. T. Foxon, Phys. Rev. Lett. **60**, 848 (1988).

[2] D. A. Wharam, T. J. Thornton, R. Newbury, M. Pepper, H. Ahmed, J. E. F. Frost, D. G. Hasko, D. C. Peacock, D. A. Ritchie, and G. A. C. Jones, J. Phys. C **21**, L209 (1988).

[3] R. Landauer, Philos. Mag. **21**, 863 (1970).

[4] M. Buttiker, Phys. Rev. Lett. **57**, 1761 (1986).

[5] M. Buttiker, Phys. Rev. B **41**, 7906 (1990).
[6] M. J. Laughton, J. R. Barker, J. A. Nixon, and J. H. Davies, Phys. Rev. B **44**, 1150 (1991).
[7] H. Sakaki, Jpn. J. Appl. Phys. **19**, L735 (1980).
[8] G. Timp, R. Behringer, S. Sampere, J. E. Cunningham, and R. E. Howard, in *Proceedings of the International Symposium on Nanostructure Physics and Fabrication*, edited by M. A. Reed and W. P. Kirk (Academic, New York, 1989), p. 331.
[9] A certain discrepancy exists in the literature concerning the calculation of the transport mean free path l_{tr}. In this work, we define $l_{tr}=\hbar k_F \mu_e/e$, where $k_F=\sqrt{2\pi n_s}$. Some reported values do not include the factor of $\sqrt{2}$ in the above equation, resulting in a reduction in l_{tr} by ~ 1.4.
[10] G. Timp, in *Semiconductors and Semimetals*, edited by M. A. Reed (Academic, New York, 1990), p. 113.
[11] J. A. Nixon, J. H. Davies, and H. U. Baranger, Phys. Rev. B **43**, 12 638 (1991).
[12] L. I. Glazman and M. Jonson, Phys. Rev. B **44**, 3810 (1991).
[13] M. Ogata and H. Fukuyama, Phys. Rev. Lett. **73**, 468 (1994).
[14] A. M. Zagoskin, S. N. Rashkeev, R. I. Shekhter, and G. Wendin, J. Phys. Condens. Matter **7**, 6253 (1995).
[15] K. Ismail, S. Washburn, and K. Y. Lee, Appl. Phys. Lett. **59**, 1998 (1991).
[16] T. Honda, S. Tarucha, T. Saku, and Y. Tokura, Jpn. J. Appl. Phys. **34**, L72 (1995).
[17] G. L. Snider, Ph.D. thesis, University of California at Santa Barbara, 1991.
[18] S. J. Koester, C. R. Bolognesi, M. Thomas, E. L. Hu, H. Kroemer, and M. J. Rooks, Phys. Rev. B **50**, 5710 (1994).
[19] C. Nguyen, B. Brar, H. Kroemer, and J. H. English, Appl. Phys. Lett. **60**, 1854 (1992).
[20] C. Nguyen, B. Brar, H. Kroemer, and J. English, J. Vac. Sci. Technol. B **10**, 898 (1992).
[21] S. Ideshita, A. Furukawa, Y. Mochizuki, and M. Mizuta, Appl. Phys. Lett. **60**, 2549 (1992).
[22] A. Furukawa, Appl. Phys. Lett. **62**, 3150 (1993).
[23] J. Shen, J. D. Dow, S. Y. Ren, S. Tehrani, and H. Goronkin, J. Appl. Phys. **73**, 8313 (1993).
[24] G. Tuttle, H. Kroemer, and J. H. English, J. Appl. Phys. **65**, 5239 (1989).
[25] J. N. Walpole and K. W. Nill, J. Appl. Phys. **42**, 5609 (1971).
[26] S. J. Koester, C. R. Bolognesi, E. L. Hu, H. Kroemer, and M. J. Rooks (unpublished).
[27] P. L. McEuen, B. W. Alphenaar, R. G. Wheeler, and R. N. Sacks, Surf. Sci. **229**, 312 (1990).
[28] Y. Wang, S. Y. Chou, and M. R. Melloch, Superlatt. Microstruct. **14**, 227 (1993).
[29] T. Bever, Y. Hirayama, and S. Tarucha, Jpn. J. Appl. Phys. **33**, L800 (1994).
[30] K. Ismail (unpublished).
[31] R. Dingle, H. L. Stormer, A. C. Gossard, and W. Wiegmann, Appl. Phys. Lett. **33**, 665 (1978).
[32] J. A. Nixon and J. H. Davies, Phys. Rev. B **41**, 7929 (1990).
[33] P. T. Coleridge, Phys. Rev. B **44**, 3793 (1991).
[34] J. A. Nixon and J. H. Davies, Superlatt. Microstruct. **9**, 187 (1991).
[35] B. J. van Wees, L. P. Kouwenhoven, H. van Houten, C. W. J. Beenakker, J. E. Mooij, C. T. Foxon, and J. J. Harris, Phys. Rev. B **38**, 3625 (1988).
[36] J. H. Davies and G. Timp (unpublished).
[37] C. R. Bolognesi, H. Kroemer, and J. H. English, J. Vac. Sci. Technol. B **10**, 877 (1992).
[38] C. R. Bolognesi, H. Kroemer, and J. H. English, Appl. Phys. Lett. **61**, 213 (1992).